Effect of Type III Antifreeze Protein Dilution and Mutation on the Growth Inhibition of Ice

Carl I. DeLuca,* Heman Chao,* Frank D. Sönnichsen,# Brian D. Sykes,# and Peter L. Davies*
*Department of Biochemistry, Queen's University, Kingston, Ontario K7L 3N6, and #Protein Engineering Network of Centres of Excellence and Department of Biochemistry, University of Alberta, Edmonton, Alberta T6G 2S2 Canada

ABSTRACT Mutation of residues at the ice-binding site of type III antifreeze protein (AFP) not only reduced antifreeze activity as indicated by the failure to halt ice crystal growth, but also altered ice crystal morphology to produce elongated hexagonal bipyramids. In general, the *c* axis to *a* axis ratio of the ice crystal increased from ~2 to over 10 with the severity of the mutation. It also increased during ice crystal growth upon serial dilution of the wild-type AFP. This is in marked contrast to the behavior of the α-helical type I AFPs, where neither dilution nor mutation of ice-binding residues increases the *c*:*a* axial ratio of the ice crystal above the standard 3.3. We suggest that the ice crystal morphology produced by type III AFP and its mutants can be accounted for by the protein binding to the prism faces of ice and operating by step growth inhibition. In this model a decrease in the affinity of the AFP for ice leads to filling in of individual steps at the prism surfaces, causing the ice crystals to grow with a longer *c*:*a* axial ratio.

INTRODUCTION

Antifreeze proteins (AFPs), of which there are at least four structurally different types in fishes (Davies and Hew, 1990), inhibit ice growth from solution (DeVries et al., 1970) and in the frozen state (Knight et al., 1984). AFPs are thought to function in these activities by an adsorption-inhibition mechanism (Raymond and DeVries, 1977). They do not physically cover the ice (Wilson et al., 1993), but break its growing surfaces into numerous microspaces between bound AFPs. When water adds to the ice lattice at these microspaces, the ice is forced to grow with a pronounced radius of curvature and hence an increase in surface free energy that translates into a lowering of the nonequilibrium freezing point (Knight et al., 1991; Cheng and DeVries, 1991; Wilson, 1993). Fish AFPs inhibit ice growth normal to the *c*-axis, thereby constraining a seed ice crystal to form a hexagonal bipyramid (DeVries, 1984). In the presence of high AFP concentrations and when the nonequilibrium freezing point has been exceeded, the extreme expression of this inhibition is spicular growth parallel to the *c*-axis (Raymond and DeVries, 1977). At the molecular level, early models of AFP action visualized AFP binding to the prism planes and forming a hexagonal bipyramid by step growth inhibition (DeVries, 1984). As the growth of each hexagonal plate is arrested, a new one emerges from the basal plane, only to be inhibited before reaching the full extent of the previous plate. In this way the crystal comes to bipyramidal points and there is no further growth at that degree of undercooling. This is in contrast to normal ice growth under mild subcooling, where the rate of growth along the *a* axis is ~100 times faster than along the *c* axis and ice grows with a circular disk-like morphology (Kallungal, 1975).

The details of the molecular interactions between AFPs and the ice lattice, however, have remained elusive. Early speculations about a hydrogen bonding match between hydrophilic residues on the α-helical type I AFP and oxygens on the prism plane (parallel or perpendicular to the *a* axis) of the ice lattice (DeVries and Lin, 1977), and about the role of the helix dipole in orienting type I AFP to this plane (Yang et al., 1988) became untenable when ice etching studies showed that different AFPs had specific planes (and even directions) along which they bind to ice (Knight et al., 1991; Cheng and DeVries, 1991). Thus whereas the highly repetitive antifreeze glycoproteins (AFGPs) do indeed appear to bind to the prism faces (or a plane very close to the prism face) (Knight et al., 1993), type I AFPs bind to a pyramidal plane defined by the Miller indices $\{20\bar{2}1\}$ in the direction $\langle 01\bar{1}2\rangle$ (Knight et al., 1991). With the knowledge that type I AFP is a single long α-helix both in solution (Ananthanarayanan and Hew, 1977; Raymond et al., 1977) and in protein crystals (Yang et al., 1988), the fitting of this antifreeze to ice has centered around the 16.5 Å spacing between the *i*, *i* + 11 threonines matching the 16.7 Å distance between accessible oxygens along the $\langle 01\bar{1}2\rangle$ direction of the $\{20\bar{2}1\}$ binding plane (Knight et al., 1991). Even with all this information and a refined x-ray structure (Sicheri and Yang, 1995), many different models have been proposed for the fit of type I AFP to ice (Wen and Laursen, 1992a; Chou, 1992; Jorgensen et al., 1993; Madura et al., 1994; Sicheri and Yang, 1995).

The problems of matching a structure to a binding plane on ice are even harder with the two globular AFPs because, unlike type I AFP and the AFGPs, AFP types II and III do not have any obvious repeating sequence motifs to help identify the ice-binding site and suggest a match to the ice

Received for publication 3 June 1996 and in final form 14 August 1996.
Address reprint requests to Dr. Peter L. Davies, Department of Biochemistry, Queen's University, Kingston, Ontario K7L 3N6, Canada. Tel.: 613-545-2983; Fax: 613-545-2497; E-mail: daviesp@post.queensu.ca.
Dr. Sönnichsen's present address is Department of Physiology and Biophysics, Case Western Reserve University, Cleveland, OH 44106-4970.

0006-3495/96/11/2346/10 $2.00

lattice (Li et al., 1985; Ng et al., 1986; Sönnichsen et al., 1993, 1995). Mutations of type III AFP have identified a cluster of residues (N14, T18, and Q44) that have an ice-binding phenotype, although there are other residues (S42 and N46) nearby whose mutation appears to have little effect on thermal hysteresis (Chao et al., 1994). To verify the identification of the ice-binding site we have made a series of mutations at A16, a solvent-accessible residue adjacent to the known ice-binding residues. The substitution of bulky side chains at this position had the predicted effect of lowering thermal hysteresis activity. Both the A16 substitutions and the previous ice-binding mutants produced a remarkable variation in ice crystal morphology. Such crystal morphology changes were not observed with type I AFP mutants that had reduced thermal hysteresis activity (Wen and Laursen et al., 1992b). We suggest that these observations on type III AFP ice-binding mutants are consistent with this antifreeze binding to the prism faces of ice and acting by the step growth inhibition model, and that the varied ice crystal morphologies result from the filling in of ice steps produced by mutants that have a reduced affinity for ice or are more easily overgrown.

MATERIALS AND METHODS

Site-directed mutagenesis

The expression vector pT7-7(f) (DeLuca et al., 1993) containing the synthetic gene for type III AFP (Chao et al., 1993) was used for the generation of single-stranded, uracil-containing template (Kunkel et al., 1987), and subsequently for protein production. The A16 mutants were derived by site-directed mutagenesis from three sets of mixed primers of the sequence

5′-CCCGATTAATACT**XYZ**CTGACTCTGGTT-3′.

The first two primer sets were designed to substitute other amino acids for A16 while minimizing retention of alanine. In set one, the proportions of bases in **X**, **Y**, and **Z** were as follows: **X** = 0.5 A and 0.5 T; **Y** = 0.1 C, 0.2 G, 0.35 A, and 0.35 T; **Z** = 0.5 G and 0.5 C. In set two, the same proportions were used for **Y** and **Z**, but **X** = 0.3 G and 0.7 C. These primer sets only encoded one of the three possible stop codons, thereby reducing the frequency of nonsense mutations. The third primer set, where **X** = T, **Y** = 0.5 A and 0.5 T, and **Z** = T, was designed to produce a Tyr or Phe substitution because neither of these mutants was produced using the other primers. All clones were verified by sequencing across the mutagenic oligonucleotide region and flanking DNA by the dideoxy method (Sanger et al., 1977) using Sequenase Ver2.0 (USB).

Production and purification of recombinant AFP

Plasmid DNAs were prepared using the Wizard miniprep DNA purification kit (Promega) and transformed into *Escherichia coli* JM 83 containing the vector pGP1-2 (Tabor and Richardson, 1985). Expression of the AFP gene was heat-induced according to Tabor (1990). Harvested cells from a 4 liter culture were frozen, thawed, and then broken by sonication in 10 mM Tris-HCl (pH 8.0), 0.1 mM EDTA, 0.1 mM phenylmethylsulfonyl fluoride (50 ml).

The *E. coli* sonicate was centrifuged at 12,000 × *g* for 30 min at 4°C. The supernatant fraction containing soluble AFP (50 ml) was acidified to pH 3.7 by the addition of 1 M sodium acetate (pH 3.7) to a final concentration of 50 mM, clarified by centrifugation, and dialyzed against 50 mM sodium acetate (pH 3.7). The sample (~60 ml) was loaded onto an S-Sepharose HP 16/10 fast protein liquid chromatography column (Pharmacia) preequilibrated in 50 mM sodium acetate (pH 3.7). Bound AFP was eluted by a linear 0–0.3 M NaCl gradient in 50 mM sodium acetate (pH 3.7) at a flow rate of 2.5 ml/min. Fractions (2.5 ml) containing AFP were dialyzed against 5 mM NH_4HCO_3 (pH 7.9) and lyophilized.

Pellets from the *E. coli* sonicate were resuspended in 8 ml of 8 M guanidine-HCl, 100 mM Tris-HCl (pH 8.5) with gentle mixing at 20°C for 1 h. The suspension was then added dropwise to 160 ml of ice-cold refolding buffer containing 50 mM K_2HPO_4 and 100 mM NaCl (pH 10.7). The mixture was dialyzed against 50 mM sodium acetate (pH 3.7), clarified by centrifugation, and purified by fast protein liquid chromatography as above.

Type I AFP preparation

Type I AFP, represented by the component HPLC-6, was purified from winter flounder serum by the method of Fourney et al. (1984).

NMR experiments

The NMR analysis of AFP mutants was performed using ~0.5 mM protein solutions in D_2O at pH 7.0 as previously described (Chao et al., 1994). One-dimensional data were acquired at 4°C, and two-dimensional data were collected at 25°C.

Antifreeze activity measurements and photomicroscopy

Thermal hysteresis, defined as the temperature difference (°C) between the melting point and the nonequilibrium freezing point of a solution, was measured using a nanoliter osmometer (Clifton Technical Physics, Hartford, NY) as described by Chakrabartty and Hew (1991). All measurements were made in 0.1 M NH_4HCO_3 (pH 7.9). Ice crystal morphology was observed through a Leitz dialux 22 microscope and recorded by a Panasonic CCTV camera linked to a JVC Super VHS video recorder. Still images were obtained from a Silicon Graphics INDY terminal using IRIS Capture version 1.2 and printed on an HP laserjet 4. For ice growth rate analysis, samples were held at a fixed degree of undercooling and images were captured at 0- and 10-min time points.

RESULTS

Measurement of thermal hysteresis as an antifreeze activity

Thermal hysteresis is defined as the difference between freezing and melting temperatures of a solution and can be measured by observing the effects of cooling and warming on a single ice crystal in an AFP solution under a microscope. Upon cooling in the presence of wild-type AFP, the nonequilibrium freezing point is marked by extremely rapid, uncontrolled growth of the ice to fill the sample well. This is referred to as the "burst point" of the crystal. Before reaching this end point the crystal remains constant in size and shape throughout the temperature change. At the melting temperature the ice crystal visably shrinks. Our experience with ice-binding mutants (Chao et al., 1994) is that many are unable to completely suppress ice crystal growth on cooling toward the nonequilibrium freezing point. As undercooling is increased there comes a point where growth can be observed as a slow, regular expansion of the crystal. Although further cooling sometimes results in a "burst

point," the more severely affected mutants do not reach this climax but continue to grow steadily as the temperature is lowered. For consistency in thermal hysteresis measurements we have defined the freezing point as the temperature at which ice crystal growth, either controlled or uncontrolled, is perceptible by eye. This effectively means that crystal growth has reached or exceeded 0.2 μm/s along any axis. Although slower growth rates can be determined by video microscopy, this technique was only used here for qualitative assessments to avoid changing the thermal hysteresis parameters previously used for describing mutants (Chao et al., 1993, 1994).

Hindrance of ice:protein interaction by the A16 mutant series

The three identified ice-binding residues of type III AFP are clustered on two adjacent β-strands with their side chains projecting toward the solvent. This hydrophilic surface is fairly flat and has no projections on or nearby it that might impede ice:protein interaction with the H-bonding side chains of N14, T18, and Q44. To probe the importance of a flat surface for ice binding, we performed a series of mutations that introduced bulky side chains at A16. Alanine 16 lies near these ice-binding residues with its methyl group exposed to the solvent. The presence of a large residue at this site could well interfere with the ability of the ice-binding residues to contact the ice lattice. If so, an effect on thermal hysteresis and/or the ice crystal morphology should be observed.

Table 1 shows the effects of seven substitutions at position 16. In each case the introduction of a larger side chain at this position decreased thermal hysteresis activity. At a concentration of 1 mg/ml the least affected mutant (A16 M) was 84% as active as wild-type AFP, whereas the most affected, (A16H), had only 25% activity. In general, amino acids with branched side chains (V, T, L, and R) were more disruptive than the straight chain amino acid (M), and the cyclic amino acids (Y and H) produced lower thermal hysteresis activities than the branched chain mutants.

Structural analysis of A16 mutants

To ensure that the effects of these mutations on thermal hysteresis were not due to perturbations of the protein fold, the A16 substitution mutants were analyzed by 1D and 2D ^{1}H-NMR. One-dimensional spectra of five of these mutants were acquired in D_2O under conditions that have been shown to facilitate solvent exchange of exposed amide protons, whereas amides involved in structurally significant hydrogen bonds are protected against deuterium exchange. A comparison of the amide regions of these mutants (Fig. 1) demonstrated that the hydrogen bonding network and hydrogen exchange dynamics of the folded protein were undisturbed, by virtue of the presence of the same resonances at comparable intensities in each mutant at similar frequency positions. Some changes in amide proton frequencies occurred, and new aromatic resonances of Y16 in A16Y (7.26 and 6.78 ppm) and H16 in A16H (7.83 and 7.26 ppm) were observed. The frequency changes seen were small and limited, although in general the 1D ^{1}H-NMR spectra (Fig. 1) differed somewhat more than with previous mutants (Chao et al., 1994). The resonance assignment and proper fold were additionally confirmed in 2D-NMR spectra. Fig. 2 presents the αCH region of 2D-^{1}H-H NOESY spectra of mutants A16T, A16H, A16R, and A16Y. Only negligible resonance frequency shifts were observed, with the exception of the mutated residues and their sequentially or sterically neigboring residues. All structurally significant dαα cross-peaks were present, including interstrand dαα (16, 44). Similarly, all chemical shifts and NOE cross-peak intensities were comparable with those of the wild-type protein (Chao et al., 1994), confirming the preservation of the β-sheet arrangement and the fold of the mutant proteins.

TABLE 1 Effect of mutations at A16 on the antifreeze activity of Type III AFP

Sample (1 mg/ml)	Thermal hysteresis (°C)	% activity
Wild type	0.38 ± 0.01	100
A16M	0.32 ± 0.01	84
A16V	0.30 ± 0.01	79
A16L	0.28 ± 0.02	73
A16T	0.28 ± 0.00	73
A16R	0.23 ± 0.02	60
A16Y	0.13 ± 0.00	33
A16H	0.10 ± 0.01	25

The effect of AFP activity mutants on ice crystal morphology

In addition to decreasing thermal hysteresis activity, the three previously characterized ice-binding residue mutations (N14S, T18N, and Q44T) had a pronounced effect on the morphology of the ice crystals. To provide a basis for comparison, ice crystals formed in the presence of 1 mg/ml AFP at 0.1°C of undercooling were photographed after 1 min (Fig. 3). The hexagonal bipyramidal ice crystals present in wild-type AFP III consistently had a ~2:1 ratio of the crystallographic *c* and *a* axes, respectively (Fig. 3 *b*). Neither the crystal size nor the *c*:*a* axial ratio changed perceptibly during this 1-min interval. However, the ice-binding mutants of Type III AFP all produced ice crystals with distinctive morphologies that differed from the wild-type 2:1 crystal axis ratio, and they all increased in size during the 1-min interval, i.e., they permitted slow growth of the ice nucleus at this low degree of undercooling within the thermal hysteresis window (Fig. 3 *c–e*). Q44T produced hexagonal bipyramidal cystals that were somewhat larger than the wild type's and were significantly elongated. The *c*:*a* ratio from an average of three crystals formed in the presence of Q44T was ~4.9. The N14S ice crystal was noticeably longer, with a *c*:*a* ratio of ~5.9. In the presence

FIGURE 1 Amide and aromatic region of 1D ^{1}H-NMR spectra of type III AFP mutants. The spectra were acquired at 4°C in D_2O at pH 7.0. Under these conditions, only slowly exchanging amide protons are observable >3 h after dissolving the proteins. Resolved resonances in the fully active type III AFP (rQAE m1.1) are labeled with their sequence number. Vertical dashed lines are used to reference amide resonance frequencies of rQAE m1.1 in the spectra of activity mutants A16H, A16 M, A16R, A16T, and A16Y. Solid lines indicate amide resonance frequency shifts of residues 43 and 15, which are more strongly affected by the mutations because of their spatial proximity.

of T18N, ice crystals grew rapidly and failed to form bipyramidal apices. However, by extrapolation from the photograph in Fig. 3 *e*, the projected *c*:*a* ratio was approximately 6.3. In contrast, the triple mutant T18N/N14S/Q44T, which had no thermal hysteresis activity at all, was unable to restrain the growth of ice. Crystals in the presence of the triple mutant grew as disks and were indistinguishable from those formed in buffer alone (Fig. 3 *a*).

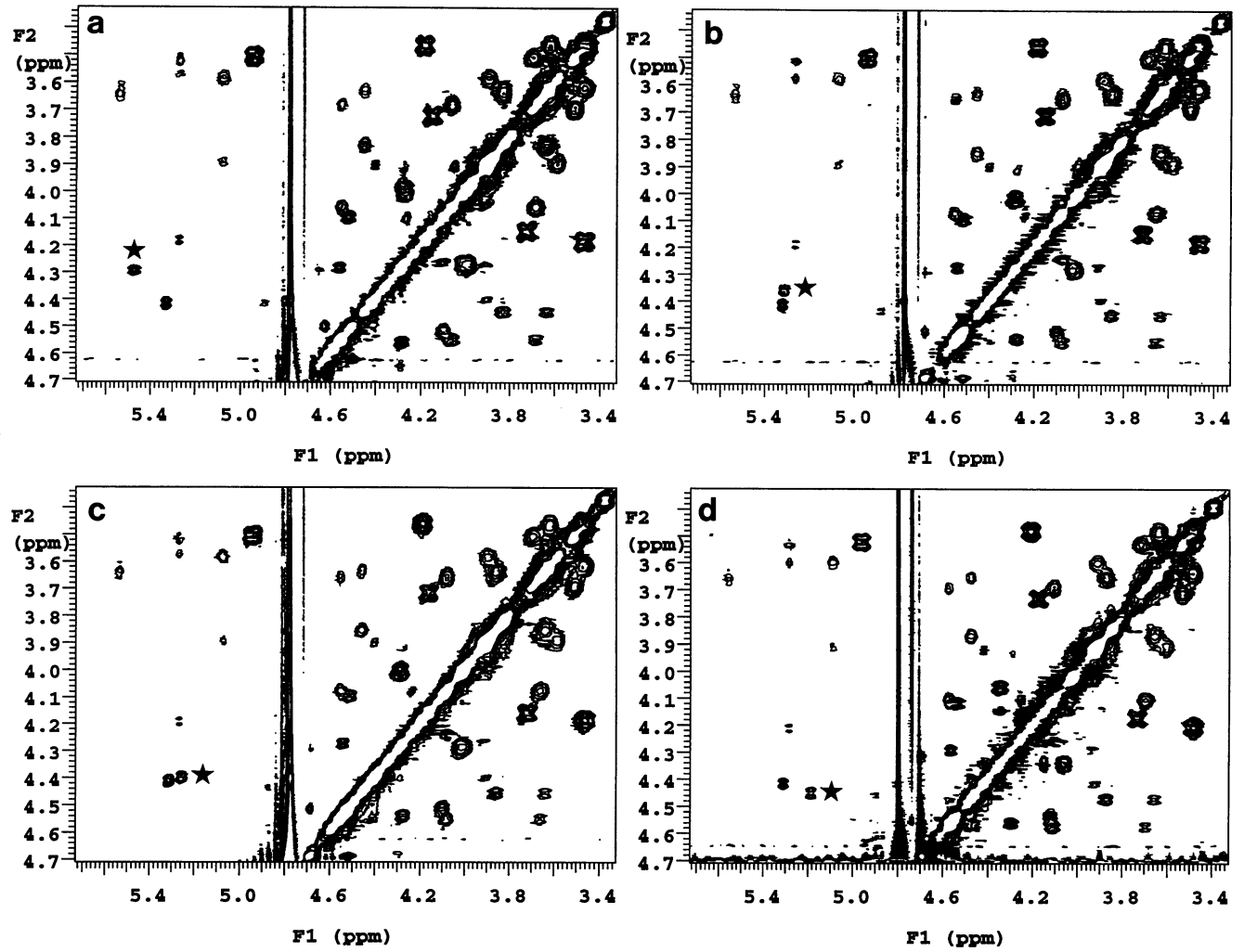

FIGURE 2 Comparison of portions of 2D-^{1}H-1H-NOESY NMR spectra of (*a*) A16T, (*b*) A16 M, (*c*) A16R, and (*d*) A16H. Spectra were obtained as described at 25°C and pH 7.0 using submillimolar protein concentrations in D_2O. The regions shown encompass intraresidue as well as structurally characteristic d$\alpha\alpha$ cross-peaks. The interstrand cross-peak between Q44 and the respective residue 16 in the mutants (d$\alpha\alpha$) is marked with a star.

There is an inverse correlation in these data between hysteresis activity and *c*:*a* axis ratio. As thermal hysteresis activity decreased (wild type, 100% > Q44T, 47% > N14S, 25% > T18N, 10%) (Chao et al., 1994), the *c*:*a* axis ratio increased (2.0 < 4.9 < 5.9 < 6.3) (Fig. 3). Thus the weaker antifreezes produced the more elongated hexagonal bipyramids.

The substitution of larger amino acids in position 16 also adversely affected the ability of the antifreeze to control ice crystal growth (Fig. 4). Ice crystals in the presence of A16 mutants all grew to differing extents when compared at zero time and after 10 min of undercooling by 0.1°C. This growth was mainly along the *c* axis, to give an increased *c*:*a* ratio over time and produce elongated crystals that were qualitatively similar to those observed for the Q44T, N14S, and T18N activity mutants. As with those ice-binding residue mutants, there was a strong correlation between the loss of thermal hysteresis activity (Table 1) and the increase in ice crystal growth (Fig. 4), with the possible exception of A16Y.

A16H produced the lowest thermal hysteresis activity of the A16 series (25% of wild type). During thermal hysteresis measurements when the temperature was reduced in steps, the seed ice crystal formed in the presence of 1 mg/ml of A16H grew steadily until the crystal reached the edges of the well. No true burst point was seen even at 0.54°C of undercooling, and the only effect of increasing the undercooling was to increase the rate of growth of the ice crystal. A16R, L, T, V, and M were qualitatively similar in their properties but formed a series of increasing antifreeze effectiveness. A16Y produced the second lowest thermal hysteresis activity of the A16 series (33% of wild type), but had a rather different effect on ice crystal morphology and burst point than the other A16 mutants. In contrast to A16H and the other A16 mutants, the ice crystal formed in the presence of 1 mg/ml of the A16Y mutant grew in sudden small

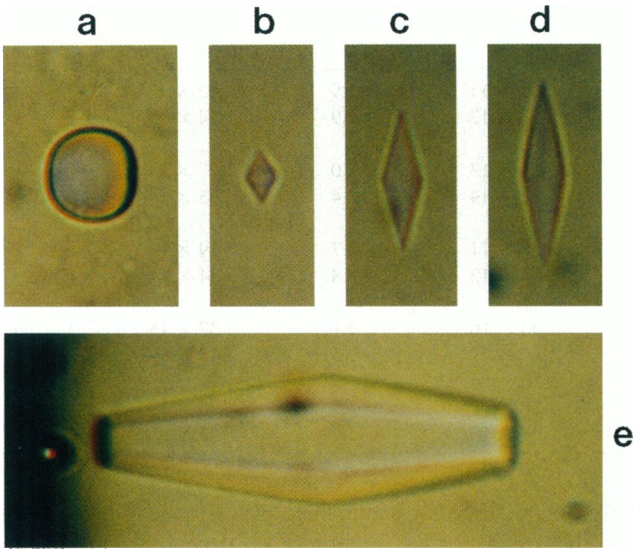

FIGURE 3 Ice crystal morphology in the presence and absence of wild-type and mutant type III AFPs. (*a*) Ice crystal formed in the presence of 0.1 M NH_4HCO_3 (pH 7.9) and photographed after undercooling by 0.1°C. (*b–f*) Ice crystals formed in the presence of 1 mg/ml of type III AFP in 0.1 M NH_4HCO_3 (pH 7.9) and photographed after 1 min of undercooling by 0.1°C, where the specific AFPs were wild type (*b*), mutant Q44T (*c*), mutant N14S (*d*), and mutant T18N (*e*).

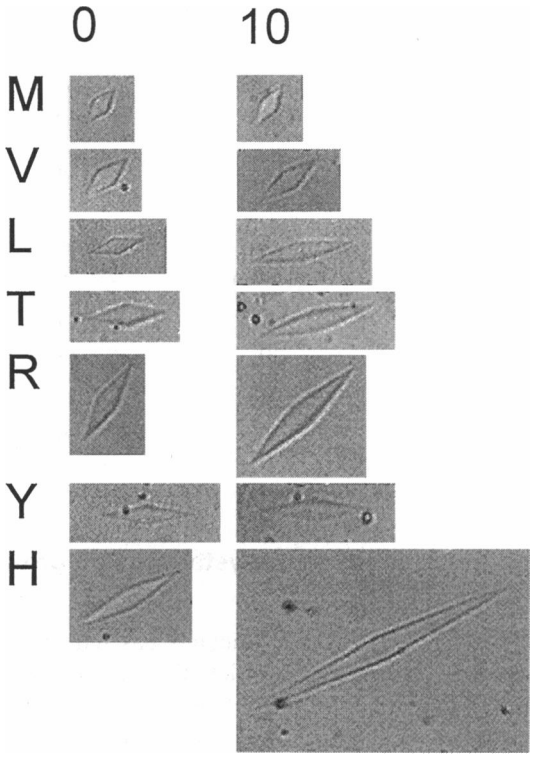

FIGURE 4 Time-lapse video microscopy of ice crystals in the presence of type III AFP A16 mutants. Ice crystals were formed in the presence of 1 mg/ml of type III AFP in 0.1 M NH_4HCO_3 (pH 7.9) with an undercooling of 0.2°C and were photographed at zero time (0) and after 10 min (10). M, L, T, V, R, Y, and H refer to the amino acid substituted for A16.

increments but stayed constant in size between these growth spurts. A burst point similar to that seen with wild-type AFP occurred at 0.22°C of undercooling. However, an alternative interpretation of this behavior could be that the small growth increments were restrained bursts and that A16Y is in fact the least active of the A16 mutants.

Effect of AFP concentration on ice crystal morphology

Activity mutants of the α-helical type I AFP and the globular type III AFP are strikingly different in their effects on ice crystal morphology. Type I AFP mutants form an ice crystal with a *c*:*a* axis ratio of ~3.3 that is essentially unchanged from the crystal obtained with the wild type (Wen and Laursen, 1992b). Activity mutants of type III AFP, as observed here, produced ice crystals with very different dimensions and shapes. Their *c*:*a* axis ratios were invariably longer than the ~2:1 ratio seen with the wild-type AFP III, and they appeared to form a continuum of ratios up to at least 10 (Fig. 4), depending on the severity of the mutation.

Mutation of the ice-binding site is one way to obtain ice growth in the presence of an AFP; dilution is another method. At low AFP concentrations and slight undercooling, ice will grow in the presence of the antifreeze (Knight et al., 1991). We therefore investigated the effect of AFP dilution on ice crystal morphology for the two antifreeze types. In each case a serial dilution was performed until an AFP concentration was reached at which ice crystals grew slowly. The dimensions of the crystals were recorded as a function of time. At a type I AFP concentration of 0.25 mg/ml and an undercooling of 0.1°C, ice crystals grew rapidly but maintained a *c*:*a* axis ratio of ~3.3 even as their volumes increased 100-fold (Table 2).

An equivalent molar concentration for type III AFP (given that its molecular weight is twice that of type I AFP) is 0.5 mg/ml. At this concentration ice growth was barely perceptible even after 10 min, and the *c*:*a* axis ratio was ~2 (Table 3). With increasing dilution down to 0.031 mg/ml (0.005 mM), ice crystal growth became more obvious and the *c*:*a* axis ratio increased up to ~3. This ratio not only increased with dilution, but also continuously increased with time during the 10-min observation.

TABLE 2 Ice crystal dimensions during growth in the presence of type I AFP

	Trial I		Trial II	
Time (min)	*c* × *a* (mm)	Ratio *c*/*a*	*c* × *a* (mm)	Ratio *c*/*a*
0	35 × 11	3.18	28 × 9	3.10
2	61 × 20	3.10	51 × 16	3.19
4	86 × 27	3.19	77 × 25	3.08
6	112 × 36	3.11	105 × 35	2.97
8	139 × 42	3.30	131 × 44	2.98

TABLE 3 Ice crystal dimensions during growth in the presence of type III AFP

Concentration (mg/ml)	Time (min)	Trial 1 (mm)	Ratio	Trial 2 (mm)	Ratio	Trial 3 (mm)	Ratio
0.5	0	18 × 9	2.0	21 × 11	1.9	22 × 12	1.8
	10	20 × 10	2.0	23 × 12	1.9	24 × 12	2.0
0.25	0	29 × 14	2.1	26 × 13	2.0	27 × 14	1.9
	10	34 × 15	2.3	34 × 14	2.4	33 × 14	2.4
0.125	0	35 × 15	2.3	30 × 11	2.7	29 × 13	2.2
	10	39 × 16	2.4	34 × 12	2.8	34 × 14	2.4
0.0625	0	30 × 13.5	2.2	33 × 16	2.1	37 × 18	2.1
	10	38 × 14	2.7	42 × 17	2.5	43 × 19	2.3
0.0313	0	33 × 15	2.2	30 × 12	2.5	36 × 15	2.4
	10	45 × 16	2.8	38 × 13	2.9	48 × 16	3.0

DISCUSSION

Effect of mutation on ice crystal growth: growth versus no growth

This analysis of type III AFP mutants has required some reevaluation of the way in which thermal hysteresis is measured and the establishment of an operational definition for this activity. Within the time course of a typical thermal hysteresis assay with wild-type AFP, the seed ice crystal shows no growth until the nonequilibrium freezing point is reached, at which point containment breaks down and the crystal grows rapidly from one or more nucleation points until the entire sample well is frozen in a matter of seconds. In contrast, ice crystals in the presence of mutant type III AFPs grow slowly but steadily, retaining their hexagonal bipyramidal shape (but with different dimensions) until the well is overgrown.

Because of this slow growth phenotype, the measurement of "thermal hysteresis activity" becomes far more subjective when mutant proteins are involved. Here and in our previous report (Chao et al., 1994), the freezing point was taken to be the temperature at which ice crystal growth of 3 μm or greater was observed over 15 s. This allowed the mutants to be ranked in terms of their effect on antifreeze activity. A more rigorous definition of antifreeze activity might actually classify these proteins as being inactive if, at high concentrations, they fail to prevent ice crystal growth. In theory, these mutants would probably not confer adequate freeze protection on an organism over long periods of undercooling unless a mechanism existed to remove ice crystals from the circulation. But in practice, natural selection has presumably acted to eliminate ineffective AFPs, and indeed in all type III AFP isoforms sequenced to date from several different species, the key ice-binding residues (N14, T18, and Q44) are invariant (Davies and Hew, 1990).

Can ice crystal growth be stopped completely, or are AFPs in effect ice retardation proteins?

This question is brought into focus when considering the effect of concentration on antifreeze activity. By the strict definition of thermal hysteresis, an AFP must completely stop the growth of ice, otherwise the freezing point has in fact been exceeded and only the rate of ice growth is being controlled. With the wild-type AFP it is possible to dilute stock solutions to the point where ice crystal growth is readily observed within the time frame of a thermal hysteresis measurement (minutes). With a much longer time frame of analysis, would there be some ice crystal growth, even in the presence of saturating concentrations of the wild-type AFP? Or is there a threshold AFP concentration above which ice growth is completely stopped, as suggested by Wen and Laursen (1992b)? Again, it could be argued that in practice natural selection acts to ensure that the concentrations of AFPs maintained by the fish are adequate to protect them from freezing at the sea water temperatures they encounter. There is evidence that this can be achieved through the modulation of AFP gene dosage (Hew et al., 1988).

Why does ice grow in the presence of AFPs?

There are at least two reasons why ice can be envisioned to grow in the presence of an AFP. At low [AFP] and low undercooling, the AFP may bind tightly to the ice surface but too sparsely to cause a significant local curvature between bound AFPs and thus inhibit water from joining the lattice. The bound AFPs would be frozen in and grown over by the ice. These are essentially the conditions used in the ice etching experiments to determine the plane and direction of binding by AFPs (Knight et al., 1991). A second explanation for ice growth would be reduced affinity for the lattice. At one extreme, the type III AFP triple mutant, N14S/T18N/Q44T, has no apparent affinity for ice, which grows in its presence as a rapidly expanding circular plate. The triple mutant does not behave differently from serum albumin or any other non-AFP in this respect. These proteins are excluded by the growing ice front. However, a mutant with reduced affinity for ice could permit ice growth by having a low but finite off rate from the lattice. Once an AFP dissociated from the surface in the presence of 55M water and undercooling, ice growth would be rapid and

might cause neighboring bound AFPs to be overgrown. In practical terms, AFP dissociation and overgrowth would both result in ice crystal growth.

Effect of mutation on ice crystal morphology

In the present study we observed that, in addition to the loss of thermal hysteresis, the ice crystal morphology formed in the presence of ice-site mutants differed from that of the wild type and reflected the severity of the mutation. Two explanations can be offered for these observations, both being a result of a loss of affinity of the protein for ice due to steric hindrance or to the misalignment of an H-bonding group. One explanation is that there are systematic alterations in step growth inhibition; the other is that type III AFP and its mutants can bind to more than one crystal plane and that mutations result in decreased affinity for one or more possible binding surfaces and hence a change in ice crystal morphology.

There is a precedent for the latter explanation. In a recent study, Chao et al. (1995) found that mixing AFP types resulted in distinct ice crystal morphologies, depending on the ratio and types of AFP that were combined. Each AFP had different preferred binding planes, as determined by the ice-etching assay of Knight et al. (1991). For the AFPs used in the mixing study, the planes of binding were $\{20\bar{2}1\}$ for type I, $\{11\bar{2}1\}$ for type II, and $\{10\bar{1}0\}$ for type III (Cheng and DeVries, 1991). The hybrid morphology of the crystals grown in the AFP mixes demonstrated that multiple binding planes can be occupied on the same crystal, and that the resulting crystal morphology was a composite of the individually bound planes.

It is not inconceivable that type III AFP has affinity for one or more binding planes in addition to the $\{10\bar{1}0\}$ plane, although for a small globular AFP the ice-binding site is of necessity compact and the protein is unlikely to be able to bind to an adsorption plane with high Miller indices. Binding to the $\{10\bar{1}0\}$ plane was suggested by ice-etching experiments at very dilute AFP concentrations because these are the conditions under which the ice hemispheres grow. Other planes of the ice might be bound by the AFP at higher concentrations. If so, mutations may differentially affect some or all of the binding planes. This could yield hybrid ice crystal morphologies, as seen with the AFP mixing experiment. However, the result that casts the most doubt on this hypothesis is the observation that for a particular activity mutant the *c:a* ratio can change continuously, at a fixed AFP concentration and degree of undercooling.

The other interpretation of the results attributes the alteration of the crystal morphology to a differential inhibition of ice plate growth. Fish AFPs inhibit ice growth by adsorbing to some aspect of the prism faces or pyramidal planes. At the molecular level the inhibition of ice growth after AFP adsorption to the surface can be explained by the Kelvin effect (Wilson, 1993). Water can still join to the lattice at the basal plane by nucleation, but as the ice spreads laterally to form a hexagonal ice plate, it becomes bound on the prism or pyramidal surfaces by AFP and its lateral growth is blocked. This leads to a tapering of the ice crystal to form bipyramidal apices. We would predict that a high concentration of a high-affinity AFP would be best at blocking the lateral spread of the ice plates before they approach the outer prism/pyramidal surface, giving rise to short crystals with a low *c:a* ratio. Dissociation or overgrowth of mutant AFPs would allow the plates to continue growth until they merge at the prism surface $\{10\bar{1}0\}$. The filling in of individual steps (or portions thereof) would average out as an increase in the *c:a* ratio (Fig. 5), and the steepness of the bipyramidal slope would reflect the severity of the AFP

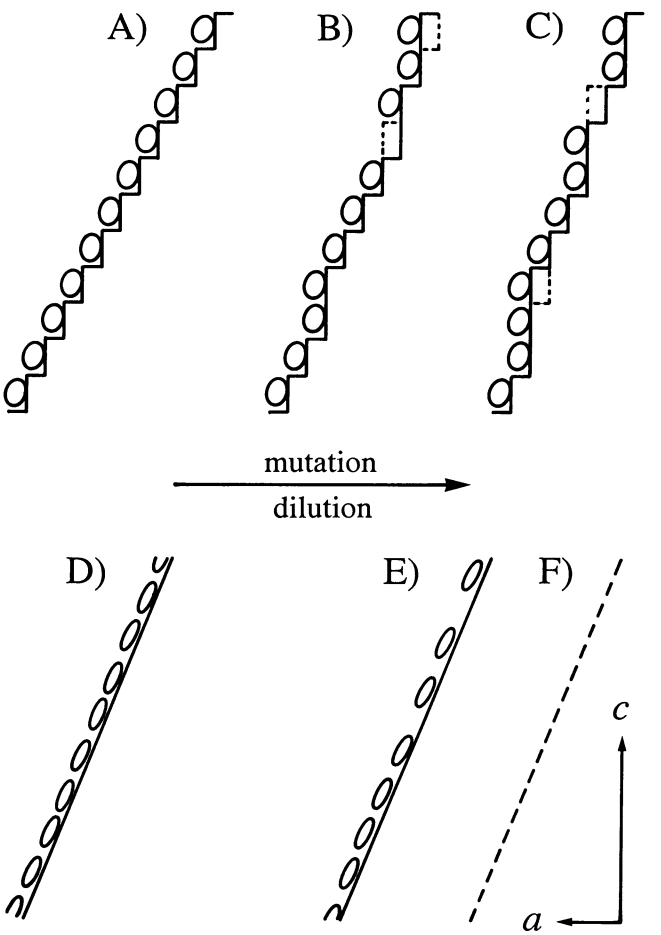

FIGURE 5 Schematic representation of the effects of AFP mutation and dilution on ice crystal morphology. The submicroscopic ice surface is shown in vertical cross section represented by solid lines, and the AFPs are indicated by circles (type III) or ovals (type I). The step diagram is stylized to illustrate the mathematical consequences of step filling on *c:a* axis ratios. In practice, the steps would be irregularly spaced, staggered, and separated by smoothly contoured ice in three dimensions. (*A–C*) Effect of type III AFP dilution or mutation on the *c:a* axis ratio, where the dotted steps represent positions recently occupied or about to be occupied by ice. (*D–F*) Effect of type I AFP dilution or mutation on the *c:a* axis ratio, where the dotted line in *F* represents the position of the pyramidal plane before ice growth. In practice, the type I AFP binding points would be irregularly spaced, staggered, and separated by smoothly contoured ice in three dimensions.

mutation. The gently tapered ice crystal obtained with A16H (25% activity) is one expression of this phenotype. Another is the flat-topped hexagonal bipyramid obtained with T18N (10% activity), where step filling in and the resultant lateral (normal to the *c* axis) expansion of the crystal occur too rapidly for bipyramidal apices to form under the experimental conditions. The extreme expression of this phenotype would tend toward the rapidly expanding disk obtained with the triple mutant (N14S/T18N/Q44T), where there is no step occupancy and the prism faces are parallel to the *c* axis.

Ice crystal growth of type I AFP and its mutants

The variation in crystal morphology with mutation is novel to type III AFP and is not seen with mutants of the long, α-helical type I AFP. For type I AFP one specific adsorption plane $\{20\bar{2}1\}$ has been proposed. Establishment of this plane would give an ice crystal with a *c*:*a* ratio of ~3.3, and this is indeed observed under the microscope during thermal hysteresis readings on this AFP. It has been suggested by several studies that the 16.5-Å spacing of repeated Thr residues can account for the specificity of this binding plane (Wen and Laursen, 1992a; Chou, 1992; Jorgensen et al., 1993; Madura et al., 1994; Sicheri and Yang, 1995). Wen and Laursen (1992b) have made numerous variants of this antifreeze. Some resulted in a decrease in thermal hysteresis activity and permitted ice crystals to grow at a higher threshold concentration of AFP. However, for all of the mutants some elements of the critical 16.5-Å spacing were preserved and the crystals grew with a constant *c*:*a* ratio of ~3.3. Because type I AFP binds to a pyramidal plane, it is not necessary to invoke step growth inhibition to account for this AFP producing hexagonal bipyramidal crystals, nor is there any evidence, based on mutation and dilution experiments, for the step growth inhibition model.

Ice crystal growth of type III AFP and its mutants

In contrast, an AFP that binds to the prism plane can only form a hexagonal bipyramid and inhibit ice crystal growth through a step inhibition mechanism. The type III AFP ice-binding site mutation phenotype, which is characterized by crystal growth with a longer *c*:*a* ratio, is consistent with both prism plane binding and step growth inhibition, with growth occurring as the steps become filled in (Fig. 5). The data in Table 3 clearly show that the *c*:*a* ratio is also a function of type III AFP concentration. Thus extreme dilution has the same effect as mutation of ice-binding residues in increasing the *c*:*a* ratio and allowing crystal growth, either because the AFP is too sparsely spaced to prevent overgrowth or because it dissociates from the ice at low AFP concentrations. In either case, water joins the lattice at the prism faces of expanding hexagonal plates, and some of the steps are filled in to produce a more steeply sided ice crystal.

In conclusion, all of the properties of AFPs described in this study, the concentration dependence of thermal hysteresis, the influence of AFPs on crystal size, morphology, and growth rate, are all reflections of the affinity of the protein for the ice surface. Although it is not possible to distinguish between irreversible binding and very low off rates for the wild-type AFP, the properties of the various ice-binding mutants might stem from different affinities for ice rather than a transition between irreversible and reversible binding.

We thank Dr. Garth Fletcher and Madonna King for the gift of winter flounder serum, and Gerry McQuaid, Sherry Gauthier, and Amber Cuthbertson for technical assistance.

This work was supported by research grants from the Medical Research Council of Canada (BDS, PLD) and the Protein Engineering Network of Centres of Excellence (BDS). HC was the recipient of an Ontario Graduate Scholarship, and CID and was supported by a Medical Research Council Studentship.

REFERENCES

Ananthanarayanan, V. S., and C. L. Hew. 1977. Structural studies on the freezing point-depressing protein of the winter flounder *Pseudopleuronectes americanus*. *Biochem. Biophys. Res. Commun.* 74:685–689.

Chakrabartty, A., and C. L. Hew. 1991. The effect of enhanced alpha-helicity on the activity of a winter flounder antifreeze polypeptide. *Eur. J. Biochem.* 202:1057–1063.

Chao, H., P. L. Davies, B. D. Sykes, and F. D. Sönnichsen. 1993. Use of proline mutants to help solve the NMR solution structure of type III antifreeze protein. *Protein Sci.* 2:1411–1428.

Chao, H., C. I. DeLuca, and P. L. Davies. 1995. Mixing antifreeze protein types changes ice crystal morohology without affecting antifreeze activity. *FEBS Lett.* 357:183–186.

Chao, H., F. D. Sönnichsen, C. I. DeLuca, B. D. Sykes, and P. L. Davies. 1994. Structure-function relationship in the globular type III antifreeze protein: identification of a cluster of surface residues required for binding to ice. *Protein Sci.* 3:1760–1769.

Cheng, C. C., and A. L. DeVries. 1991. The role of antifreeze glycopeptides and peptides in the freezing avoidance of cold-water fish. *In* Life Under Extreme Conditions. G. di Prisco, editor. Springer-Verlag, Berlin. 1–14.

Chou, K.-C. 1992. Energy-optimized structure of antifreeze protein and its binding mechanism. *J. Mol. Biol.* 223:509–517.

Davies, P. L., and C. L. Hew. 1990. Biochemistry of fish antifreeze proteins. *FASEB J.* 4:2460–2468.

DeLuca, C. I., P. L. Davies, J. A. Samis, and J. S. Elce. 1993. Molecular cloning and bacterial expression of cDNA for rat calpain II 80 kDa subunit. *Biochim. Biophys. Acta.* 121:81–93.

DeVries, A. L. 1984. Role of glycopeptides and peptides in inhibition of crystallization of water in polar fishes. *Philos. Trans. R. Soc. Lond. Biol.* B304:575–588.

DeVries, A. L., S. K. Komatsu, and R. E. Feeney. 1970. Chemical and physical properties of freezing point-depressing glycoproteins from Antarctic fishes. *J. Biol. Chem.* 245:2901–2908.

DeVries, A. L., and Y. Lin. 1977. Structure of a peptide antifreeze and mechanisms of absorption to ice. *Biochim. Biophys. Acta.* 495:380–392.

Fourney, R. M., G. L. Fletcher, and C. L. Hew. 1984. Heterogeneity of antifreeze polypeptides from the Newfoundland winter flounder *Pseudopleuronectes americanus*. *Can. J. Zool.* 62:28–33.

Hew, C. L., N. C. Wang, S. Joshi, G. L . Fletcher, G. K. Scott, P. H. Hayes, B. Buettner, and P. L. Davies. 1988. Multiple genes provide the basis for antifreeze protein diversity and dosage in the ocean pout, *Macrozoarces americanus*. *J. Biol. Chem.* 263:12049–12055.

Jorgensen, H., M. Mori, H. Matsui, M. Kanaoka, H. Yanagi, Y. Yabusaki, and Y. Kikuzono. 1993. Molecular dynamics simulation of winter floun-

der antifreeze protein variants in solution: correlation between side chain spacing and ice lattice. *Protein Eng.* 6:19–27.

Kallungal, J. P. 1975. The growth of single ice crystals parallel to the *a*-axis in subcooled quiescent and flowing water. Ph.D. dissertation, Syracuse University.

Knight, C. A., C. C. Cheng, and A. L. DeVries. 1991. Adsorption of α-helical antifreeze peptides on specific ice crystal surface planes. *Biophys. J.* 59:409–418.

Knight, C. A., A. L. DeVries, and L. D. Oolman. 1984. Fish antifreeze protein and the freezing and recrystallization of ice. *Nature.* 308: 295–296.

Knight, C. A., E. Driggers, and A. L. DeVries. 1993. Adsorption to ice of fish antifreeze glycopeptides 7 and 8. *Biophys. J.* 64:252–259.

Kunkel, T. A., J. D. Roberts, and R. A. Zarkour. 1987. Rapid and efficient site-specific mutagenesis without phenotypic selection. *Methods Enzymol.* 154:367–382.

Li, X-M., K-Y. Trinh, C. L. Hew, B. Buettner, J. Baenziger, and P. L. Davies. 1985. Structure of an antifreeze polypeptide and its precursor from the ocean pout, *Macrozoarces americanus*. *J. Biol. Chem.* 260: 12904–12909.

Madura, J. D., A. Wierzbicki, J. P. Harrington, R. H. Maughon, J. A. Raymond, and C. S. Sikes. 1994. Interactions of the D- and L-forms of winter flounder antifreeze peptide with the {201} planes of ice. *J. Am. Chem. Soc.* 116:417–418.

Ng, N. F., K. Y. Trinh, and C. L. Hew. 1986. Structure of an antifreeze polypeptide precursor from the sea raven, *Hemitripterus americanus*. *J. Biol. Chem.* 261:15690–15695.

Raymond, J. A., and A. L. DeVries. 1977. Adsorption inhibition as a mechanism of freezing resistance in polar fishes. *Proc. Natl. Acad. Sci. USA.* 74:2589–2593.

Raymond, J. A., W. Radding, and A. L. DeVries. 1977. Circular dichroism of protein and glycoprotein fish antifreeze. *Biopolymers.* 16:2575–2578.

Sanger, F., S. Nicklen, and A. R. Coulson. 1977. DNA sequencing with chain-terminating inhibitors. *Proc. Natl. Acad. Sci. USA.* 74:5463–5467.

Sicheri, F., and D. S. C. Yang. 1995. Ice-binding structure and mechanism of an antifreeze protein from winter flounder. *Nature.* 375:427–431.

Sönnichsen, F. D., B. D. Sykes, H. Chao, and P. L. Davies. 1993. The nonhelical structure of antifreeze protein type III. *Science.* 259: 1154–1157.

Sönnichsen, F. D., B. D. Sykes, and P. L. Davies. 1995. Comparative modeling of the three-dimensional structure of type II antifreeze protein. *Protein Sci.* 4:460–471.

Tabor, S. 1990. Expression using the T7 RNA polymerase/promoter system. *In* Current Protocols in Molecular Biology. F. M. Ausubel, R. Brent, R. E. Kingston, D. D. Moore, J. G. Seidman, J. A. Smith, and K. Struhl, editors. Greene Publishing and Wiley-Interscience, New York. 16.2.1–16.2.11.

Tabor, S., and C. C. Richardson. 1985. A bacteriophage T7 RNA polymerase/promoter system for controlled exclusive expression of specific genes. *Proc. Natl. Acad. Sci. USA.* 82:1074–1078.

Wen, D., and R. A. Laursen. 1992a. A model for binding of an antifreeze polypeptide to ice. *Biophys. J.* 63:1659–1671.

Wen, D., and R. A. Laursen. 1992b. Structure-function relationships in an antifreeze polypeptide. *J. Biol. Chem.* 267:14102–14108.

Wilson, P. W. 1993. Explaining thermal hysteresis by the Kelvin effect. *Cryo-Lett.* 14:31–36.

Wilson, P. W., D. Beaglehole, and A. L. DeVries. 1993. Antifreeze glycopeptide adsorption on single crystal ice surfaces using ellipsometry. *Biophys. J.* 64:1878–1884.

Yang, D. S. C., M. Sax, A. Chakrabartty, and C. L. Hew. 1988. Crystal structure of an antifreeze polypeptide and its mechanistic implications. *Nature.* 333:232–237. (Correction *Nature.* 333:503.)